Soil Dynamics and Earthquake Engineering 176 (2024) 108290

Contents lists available at ScienceDirect

Soil Dynamics and Earthquake Engineering

journal homepage: www.elsevier.com/locate/soildyn

Reliability analysis of two archetype RC buildings with hysteretic dampers

Eleonora Bruschi, Virginio Quaglini *

Politecnico di Milano, Department of Architecture, Built Environment and Construction Engineering, Piazza Leonardo da Vinci 32, 20133, Milan, Italy

A R T I C L E I N F O

Keywords:
Hysteretic dampers
Non-linear dynamic analysis
RC structures
Ductility factor
Structural reliability

A B S T R A C T

The manuscript deals with a study on the performance/reliability analysis of steel hysteretic dampers designed for the seismic retrofit of RC frame structures at the Basic Design Earthquake, BDE (characterized by a 10 % probability of being exceeded over the reference lifespan, V_R) for higher hazard levels, represented by a Maximum Considered Earthquake, MCE, with either 5 %/V_R or 2.5 %/V_R exceedance probabilities. Indeed, seismic codes prescribe that anti-seismic devices designed to satisfy the performance requirements at the BDE must be able to resist earthquakes of higher intensity. Therefore, γ-factors amplifying the design displacement or force must be considered for the design of the device capacity.

The objective of the study consists in evaluating the over-demand caused on the steel dampers incorporated in dissipative bracing systems when passing from the BDE to the two higher hazard levels, and comparing this over-demand to the values of the corresponding γ-factors proposed in current codes. Dampers with various ductility factors are considered to include the majority of current hysteretic devices.

The amplification factors recommended in the codes for hysteretic dampers are shown to be not suitable for guaranteeing the damper reliability; moreover, a dependence of the reliability of the retrofitted structures upon the ductility of the damped braces is highlighted.

1. Introduction

Seismic mitigation design, based on techniques such as energy dissipation and base isolation, is aimed at preventing structural damage, increasing life-safety and achieving a desired level of performance [1–8]. The successful implementation of these techniques was made possible by the progress in the technology of anti-seismic devices, such as hysteric and hydraulic dampers, and isolation bearings [9]. The design of anti-seismic devices is regulated by current seismic codes [10–13], which prescribe that the anti-seismic devices must be designed to satisfy the structural safety requirements to protect the life of the occupants [14–21] under the effects of the design seismic action, and must be also able to resist to earthquakes of higher intensity. For example, for seismic isolation systems, the required increased reliability is achieved by accounting, during the dimensioning, for a factor γ_x on the seismic displacement, that counts 1.2 in case of use in buildings [9], and 1.5 for use in bridges [11]. For seismic dissipation devices, or dampers, the European standard on anti-seismic devices EN 15129 [13] recommends applying to the seismic action effects a γ_x factor equal to, or greater than 1 depending on the role of the damper in the stability of the construction after the earthquake. Indeed, dampers and isolators may exhibit a brittle collapse behavior, triggering the collapse of the whole system [22]. For this reason, it is of paramount importance to control their probability of failure during extreme earthquakes and guarantee a satisfactory performance even under strong actions, as dealt e.g., in the suggested references [22–25].

While the effectiveness of the reliability factors for isolation systems recommended in the codes [10,11] has been investigated in other studies [26], the present work focuses on hysteretic dampers, a popular technology of energy dissipation systems mainly used in ordinary structures such as residential, school and industrial buildings, thanks to their viability and affordable cost [1,3,7,14–21]. The EN 15129 [13], which is compulsory for CE Marking, requires that hysteretic dampers (denoted in the standard as Displacement Dependent Devices, DDD) must be designed to sustain a maximum displacement $\gamma_x \cdot \gamma_b \cdot d_{bd}$, where d_{bd} is the design seismic displacement, $\gamma_b \geq 1.1$ is a partial factor specific for DDD, and γ_x is the reliability factor for base isolation devices that must be taken into account when the damper is used in combination with them [13]. On the other hand, in case the dampers are inserted in a bracing system and do not supplement any isolation system, $\gamma_x = 1$, and only the amplification factor $\gamma_b = 1.1$ applies. More conservative figures are provided in other codes; for example, the Italian Building Code (hereinafter referred to as NTC 2018 [12]) prescribes that dampers must

* Corresponding author.
E-mail addresses: eleonora.bruschi@polimi.it (E. Bruschi), virginio.quaglini@polimi.it (V. Quaglini).

https://doi.org/10.1016/j.soildyn.2023.108290
Received 27 July 2023; Received in revised form 3 October 2023; Accepted 10 October 2023

Symbols

b	strain-hardening ratio
CR_1	curvature degradation parameter
CR_2	curvature degradation parameter
cu	functional class
C_u	coefficient according to Table 2.4.II of NTC 2018 [12].
d_b	diameter of longitudinal reinforcement
d_{bd}	design seismic displacement of the damper
d_{max}	maximum displacement at each story of the buildingd_p performance displacement
d_u	ultimate displacement of the damper
d_y	yield displacement of the damper
f_c	compressive strength of concrete
f_y	yield stress of longitudinal steel reinforcement
h	overall depth of beam or column
K_B	elastic stiffness of the brace
K_D	elastic stiffness of the damper
K_{DB}	stiffness of the damped bracing system
I_{eq}	effective area moment of inertia of beam or column
I_g	gross area moment of inertia of beam or column
L_{pl}	plastic hinge length
$M_{E_{yd}}$	acting bending moment around the local axis y
$M_{E_{zd}}$	acting bending moment around the local axis z
$M_{R_{yd}}$	yield bending moment around the local axis y
$M_{R_{zd}}$	yield bending moment around the local axis z
N_{E_d}	applied axial force
$N_{R_{cd}}$	resisting axial force
PGA	Peak Ground Acceleration
R_0	initial value of the curvature parameter
SF	scale factor
T_R	return period
V_{dbd}	maximum output force of the damper
V_N	nominal life of a structure
V_R	reference life of a structure
z	distance from critical section of maximum curvature and the element point of contraflexure
α	exponent of equation [4.1.19] of NTC 2018 [12].
$\beta_1 = \frac{d_{bd,975years}}{d_{bd,475years}}$	damper displacement amplification for CLS1
$\beta_2 = \frac{d_{bd,1950years}}{d_{bd,475years}}$	damper displacement amplification for CLS2
γ_b	amplification factor of hysteretic dampers [13].
γ_x	reliability factor [13].
ξ_{DB}	damping capacity of the damped bracing system
μ_D	damper ductility
μ_{DB}	ductility of the damped bracing system

be designed at the Life-Safety Limit State (Basic Design Earthquake, BDE, characterized by an exceedance probability of 10 % over the reference period, V_R, for the structure), but verified at the Non-Collapse Limit State (Maximum Considered Earthquake, MCE, with an exceedance probability of 5 % over V_R), where the effects of the design seismic action are amplified by a factor 1.2. The American Standard for the retrofit of existing buildings ASCE/SEI 41–2017 [27] requires that energy dissipation devices must be capable of sustaining displacements equals to either 130 % or 200 % of the seismic design displacement, depending on the number of the devices installed within each story and each direction of the building. Specifically, the 200 % factor applies in the case that less than four energy dissipation devices are installed in a given story along one principal direction of the building, otherwise a 130 % amplification can be used.

In the literature, the performance of structures equipped with either dampers or isolators under design conditions and the effectiveness of different systems has been widely investigated [28–36], but there is less information about their behavior up to MCE. The performance of isolated structures near collapse conditions and for high seismic intensities has been investigated in the last years by different researchers, as reported in Refs. [4,37–47], but, on the contrary, similar studies on structures provided with energy dissipation systems are very few. Scozzese et al. [22] performed a parametric investigation considering two steel structures of 3 and 9 floors respectively, retrofitted with fluid viscous dampers characterized by either linear or non-linear behavior. A wide range of γ-values recommended in international seismic codes (e.g. Refs. [13,27]) was considered for the design of the damper capacity. The investigation focused on the consequences of the failure of the dampers, due to the exceeding of either their force or displacement capacity, on the seismic performance and the structural robustness of the two structures. The study highlighted that γ-factors not less than 3 should be used to achieve low failure probabilities. Moreover, referring to medium and high-rise buildings, the use of different γ-factors was suggested at different floors, by tailoring the values to the specific properties of the dampers employed at each story. Similar contributions on the reliability of structures equipped with steel hysteretic dampers can be found in Refs. [48,49].

The aim of the paper is to present a preliminary study to identify critical aspects of the reliability of hysteretic dampers in limiting building damage under extreme seismic actions and to provide the basis for implicit risk assessment considering possible over-demand of the dampers. Specifically, the performance/reliability of steel hysteretic dampers, designed for the seismic retrofit of reinforced concrete (RC) frame structures at the Life Safety Limit State according to the Italian Building Code [12], is investigated for higher hazard levels, represented by a Maximum Considered Earthquake with either 5 %/V_R or 2.5 %/V_R exceedance probabilities. Two archetype RC frames of 3 and 6 stories, respectively, are retrofitted with hysteretic dampers in order to guarantee the Immediate Occupancy structural performance, i.e., the condition in which the structure, after the earthquake, is immediately accessible as it retains its original strength and stiffness [4]. The seismic performance and the structural reliability of the upgraded structures under higher intensity earthquakes are assessed by checking the absence of structural collapse and the consistency of the over-demand of the damper system with the capacity designed according to the codes. Different design solutions are investigated in a parametric study, exploring DDDs characterized by various ductility factors and stiffness values.

The retrofit design is performed by applying a procedure ([14–17]) based on the Capacity Spectrum Method. This methodology exploits analytical equations to distribute the stiffness and strength of the dissipation braces at every floor of the building with the target of matching the lateral deformation of the retrofitted frame to the first mode deformation of the as-built frame, in order to ensure the simultaneous engagement of all the dampers [6]. Therefore, this study is valid primarily for low-rise and mid-rise structures regular in plan and in elevation, for which the lateral deformation is essentially governed by the first mode, whereas it is not suitable for structures where the contribution of higher modes is not negligible. This aspect does not represent a critical limitation from a practical point, given that in many countries, (e.g., Italy), the largest part of the existing building stock consists of low-rise and medium-rise buildings [14,50]. Examples include residential buildings, schools, industrial sheds etc., for which the use of hysteretic dampers is normally preferred [1,3,6]. Moreover, the study conducted by Scozzese et al. [22] showed worse results in terms of system reliability levels of the 9-story case-study building compared to the 3-story case-study; in particular, non-uniform failures among dampers of different stories were observed. The Authors [22] ascribed this behavior to the design method adopted for the retrofit which was carried out based on the first mode response approximation (similar to the approach adopted in the present work) which is less accurate for the high-rise buildings.

2. Description of the case-study structures

The study is performed by considering as archetypes of residential RC buildings the two examples reported in Ref. [51], which consist of a 3- and a 6-story moment-resisting frames with a rectangular plan of 25 × 15 m^2 and bays of 5 m in each horizontal direction, as shown in Fig. 1. Both structures are designed according to the NTC 2018 [12], which provides a similar approach to the Eurocode 8 [10], for a moderate seismicity area characterized by PGA = 1.91 m/s^2 and soil type B, considering a low ductility class (Class B). Sketches of the building, with the main dimensions in plan and in elevation are reported in Figs. 1 and 2, while column and beam reinforcement is listed in Table 1. C25/30 concrete and B450C steel [12] for reinforcement are assumed.

A 20 cm thick reinforced concrete slab supporting a 5 cm screed (0.95 kN/m^2), flooring (0.4 kN/m^2) and partition walls (1.6 kN/m^2) are considered as permanent non-structural loads for intermediate floor slabs. According to the NTC 2018 [12], the assumed live loads are equal to 2 kN/m^2 corresponding to residential use. Additional design information is reported in Ref. [51].

Both structures are designed to fail in flexure, thus other failure mechanisms (such as shear failure of beams, columns or beam-column joints, bond slip and low-cycle fatigue, etc.) are out of the scope of the work.

3. Retrofit design of the case-study structures

The two buildings are upgraded to withstand seismic action effects corresponding to a high seismic area, simulating e.g., an update to the hazard maps and/or code regulations. The retrofit design is performed by assuming the seismic loads provided by the NTC 2018 [12] for Life-Safety Limit State (LLS), considering two sites in southern Italy, Benevento (Long 14.787°, Lat 41.1305°) and Tramutola (Long 15.7919°, Lat 40.3176°), belonging to seismic zone 1 according to the old national seismic classification [52]. By assuming a typical residential building use, ordinary structure with nominal life V_N = 50 years, functional class cu = II corresponding to C_u = 1.0, the resulting reference life of the two structures is V_R=V_N·C_u = 50 years. A topography condition T_1 is assumed, while soil type B (deposits of very dense sand, gravel, or very stiff clay) for Benevento and soil type C (deep deposits of dense or medium-dense sand, gravel or stiff clay) for Tramutola are considered. The resulting PGAs are equal to 2.94 m/s^2 (Benevento) and 3.41 m/s^2 (Tramutola), respectively. The present work is developed as a pilot study; therefore, the investigation is restricted to two sites only, but it will be extended in the future to other sites, with different topographies and soil conditions, to provide a general validity to this research.

Diagonal steel braces equipped with hysteretic dampers (hereinafter called as "damped braces") are installed in the facades (4 units at each floor in both X and Z direction), according to the layout shown in Fig. 3.

Similarly to other studies [5,14–17] and [20], the behavior of the devices is assumed as elastic-perfectly plastic with bilinear force-displacement curve as shown in Fig. 4, where V_y is the maximum force, d_{bd} is the seismic displacement, d_u is the ultimate displacement, K_D is the initial or elastic stiffness and μ_D is the ductility factor of the damper, defined as the ratio between the seismic displacement d_{bd} and the yield displacement d_y. For the analyses performed in the study, it is assumed that the damper is provided with sufficient capacity d_u to accommodate the displacement demand at each hazard level.

The damped brace is an in-series system whose properties depend on the properties of the linear elastic brace (B) and those of the elasto-plastic damper (D); the stiffness K_{DB}, ductility μ_{DB} and damping capacity ξ_{DB} of the single damped brace (DB) are determined through Eqs. (1)–(3):

$$K_{DB} = \frac{K_D K_B}{K_D + K_B} \tag{1}$$

$$\mu_{DB} = 1 + \frac{\mu_D - 1}{1 + K_D/K_B} \tag{2}$$

$$\xi_{DB} = \frac{2}{\pi} \bullet \frac{(\mu_{DB} - 1)}{\mu_{DB}} \tag{3}$$

where K_B/K_D is the ratio between the stiffnesses associated to the steel brace K_B and the damper K_D, respectively, and is taken ≥2 in order to guarantee that the largest part of the deformation of the story is concentrated in the damper, enhancing the amount of energy dissipation [22,53]. Table 2 lists the values of μ_{DB} and ξ_{DB} considered in the study, which cover typical values of μ_D [5,14–16,21] and [54], and K_B/K_D ratio

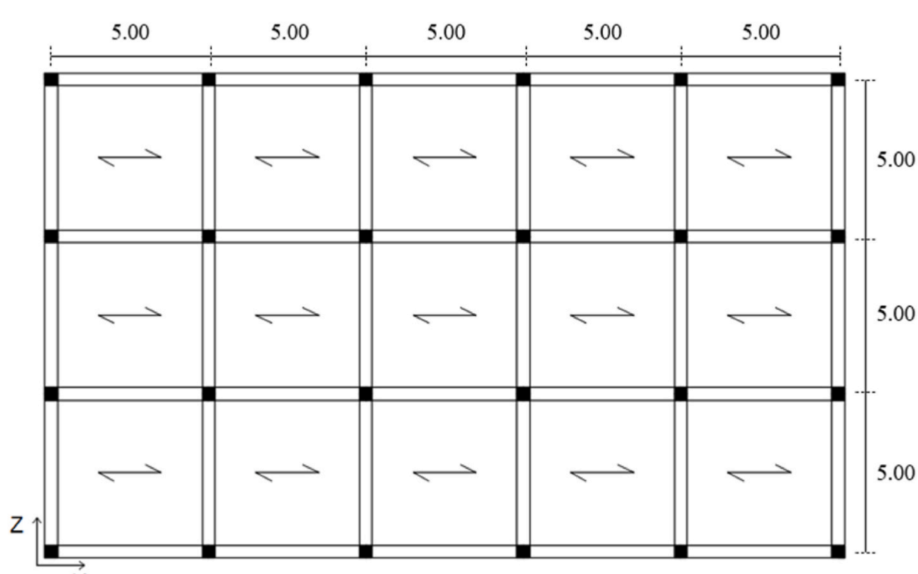

Fig. 1. Plan view of the two case-study structures (dimensions in meters).

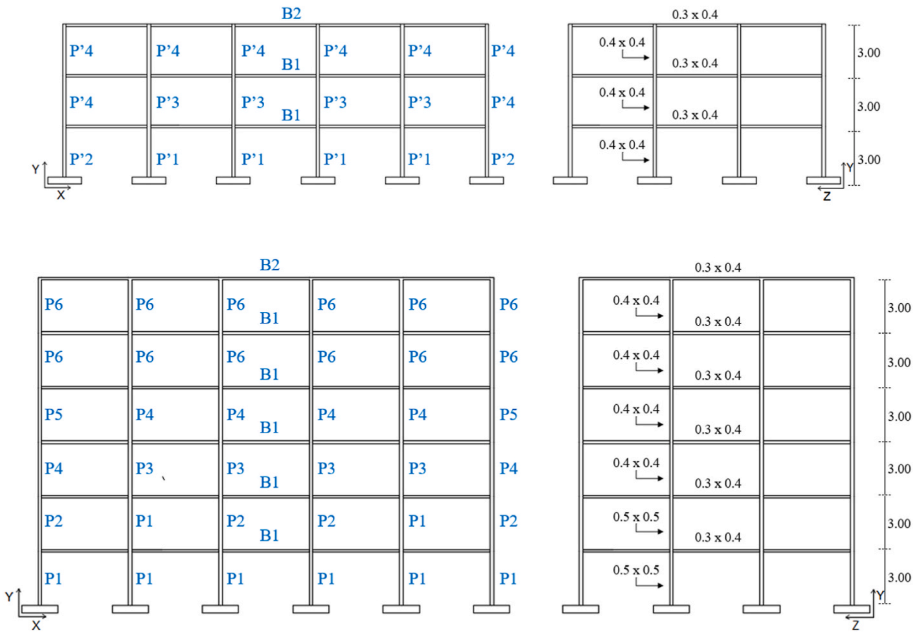

Fig. 2. Elevation view of the case-study structures and typical cross-sections of beams and columns (dimensions in meters).

Table 1
Reinforcement details of beams and columns according to the nomenclature of Fig. 2.

ID	Longitudinal reinforcement (top + bottom bars)	Transverse reinforcement (stirrups dimension/spacing at beam-column joint)
P'1	8φ18	φ10/5 cm
P'2	8φ18	φ10/8 cm
P'3	8φ18	φ10/10 cm
P'4	8φ18	φ10/12.5 cm
P1	12φ18	φ12/5 cm
P2	12φ18	φ12/8 cm
P3	8φ18	φ12/5 cm
P4	8φ18	φ12/8 cm
P5	8φ18	φ12/10 cm
P6	8φ18	φ12/12.5 cm
B1	4φ16 + 2φ16	φ8/8 cm
B2	3φ16 + 2φ16	φ8/8 cm

[5,14,17,20] and [21] for devices on the market today.

The size of the dampers was calculated by applying the Direct Displacement-Based Design (DDBD) retrofit procedure developed by the Authors of this work [14–17]. In the present work, the design target displacement d_p is defined in agreement with reference [4] as the ending point of the elastic branch of the capacity curve along either horizontal direction, as shown in Fig. 5. This assumption corresponds to the Immediate Occupancy (IO) performance level [4], which guarantees that the structure is immediately accessible after a main earthquake, since the strength and the stiffness of the structural elements are not compromised. The damping system is designed to achieve the IO performance for a return period T_R of 475 years, corresponding to a probability of non-exceedance of 10 % for a nominal life V_N of 50 years of an ordinary building with use class cu = II (LLS according to NTC 2018 [12]).

It is worth noting that, according to the adopted procedure, the damper ductility factor μ_D is assigned by the designer, and the design displacement d_{bd} is determined by the target displacement d_p of the building; therefore, also by referring to Fig. 4, the damper properties which are defined by the retrofit design procedure are the yield displacement $d_y = d_{bd}/\mu_D$ and the yield force V_y.

4. Numerical model in OpenSees

Full 3-D numerical models of the structures are formulated in the OpenSees framework [55,56]. Beams and columns are modelled using the *forceBeamColumn* element object [57], in the form of the *beamWithHinges* element [56], assigning a linear elastic material behavior to the internal sub-element, and a non-linear behavior to the two external sub-elements. The length of the external sub-elements is defined as the length of the plastic hinge L_{pl} evaluated by Eq. (4) in accordance with the Eurocode 8 [58], and assuming a well-detailed confinement model of concrete [59,60]:

$$L_{pl} = \frac{z}{30} + 0.2h + 0.11\left(\frac{d_b f_y}{\sqrt{f_c}}\right) \tag{4}$$

In these two regions, the concrete non-linear behavior is modelled through a fiber section model, where each steel bar corresponds to a single fiber, using uniaxial Giuffre-Menegotto-Pinto constitutive law [61], equivalent to *Steel02* material model with isotropic strain hardening [62]. The strain-hardening ratio b is assumed equal to 0.005, as specified in Ref. [51]. The parameters that control the transition from the elastic to the plastic branch are $R_0 = 18$, $C_{R1} = 0.925$ and $C_{R2} = 0.15$ [56]. The concrete model is implemented using the library uniaxial material *Concrete04*, which is based on the model proposed by Popovics [63]; the properties of the core region of the sections are evaluated referring to Equations (A6 – A8) of the Eurocode 8 [58] and the tensile strength of concrete is neglected in both core and cover regions [59,64]. It is worth mentioning that the material properties of the building are evaluated disregarding the confidence factors for existing structures [12, 58]. In order to account for concrete cracking, an effective area moment of inertia I_{eq}, equal to 50 % of the gross area moment of inertia I_g is assigned to the interior elastic sub-element, according to the provisions of the Italian and the European norms [12,58].

The modelling approach is consistent with the design code adopted [12] and has been demonstrated to reproduce, with enough accuracy, the seismic response of RC members characterized by flexural behavior [59,60].

In the model, the masses of the structural members (beams, columns, and slabs) are concentrated at the center of mass of each floor; dead and live loads are uniformly distributed on the beams according to the

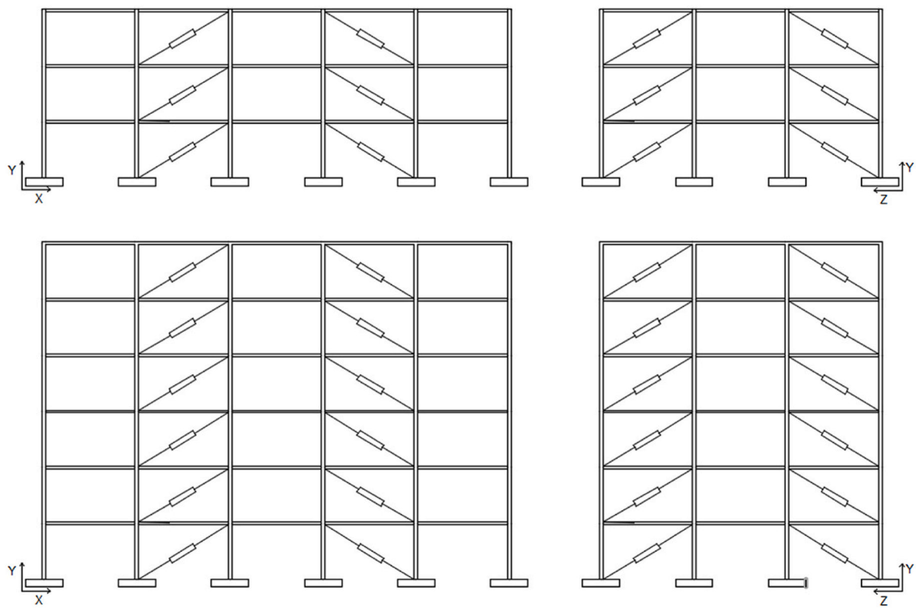

Fig. 3. Diagonal layout of steel braces equipped with hysteretic dampers for case-study buildings.

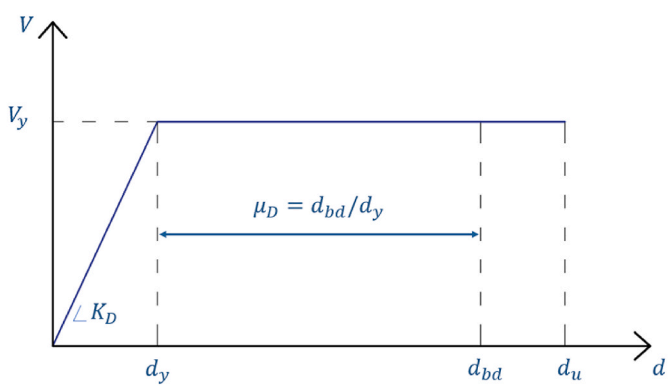

Fig. 4. Elastic-perfectly plastic force-displacement curve assumed for the dampers.

Table 2
Values of μ_{DB} and ξ_{DB} of damped braces for different values of μ_D and K_B/K_D.

μ_D (–)	$K_B/K_D = 2$		$K_B/K_D = 3$		$K_B/K_D = 4$		$K_B/K_D = 5$	
	μ_{DB} (–)	ξ_{DB} (%)	μ_{DB} (–)	ξ_{DB} (%)	μ_{DB} (–)	ξ_{DB} (%)	μ_{DB} (–)	ξ_{DB} (%)
4	**3.0**	*42.4*	**3.3**	*44.1*	**3.4**	*44.9*	**3.5**	*45.5*
6	**4.3**	*49.0*	**4.8**	*50.3*	**5.0**	*50.9*	**5.2**	*51.3*
8	**5.7**	*52.4*	**6.3**	*53.5*	**6.6**	*54.0*	**6.8**	*54.3*
10	**7.0**	*54.6*	**7.8**	*55.4*	**8.2**	*55.9*	**8.5**	*56.2*
12	**8.3**	*56.0*	**9.3**	*56.8*	**9.8**	*57.2*	**10.2**	*57.4*
14	**9.7**	*57.1*	**10.8**	*57.7*	**11.4**	*58.1*	**11.8**	*58.3*
16	**11.0**	*57.9*	**12.3**	*58.5*	**13.0**	*58.8*	**13.5**	*58.9*

tributary area concept; P-Delta effects are considered in the analysis, while bond slip and low-cycle fatigue effects are disregarded. The columns at the ground floor have fixed base supports, simulating rigid foundations. The damping of the frame is defined according to the Rayleigh method, as a function of the tangent stiffness matrix only, assuming a 5 % viscous damping ratio (as indicated in Ref. [51]), to take into account the energy dissipation coming from infill panels and other non modelled non-structural components [59].

The floor slabs are modelled as rigid diaphragms, by constraining the nodes belonging to the same floor to have the same displacement. "Axial buffers" [64] are introduced in the FE model through a *zeroLength* element object [65] characterized by a virtually zero axial stiffness and very high stiffnesses in shear and bending, placed between one end of each beam and the adjacent node belonging to the rigid diaphragm. This element works as an axial release to eliminate the fictitious axial force generated by the interaction between beam elements modelled with fiber sections and the rigid diaphragm [64].

The braces equipped with the hysteretic damper are modelled as truss elements [56] with an associated *uniaxialMaterial* model with elastic-perfectly plastic behavior [65].

5. Seismic input

The seismic action is defined in accordance with the NTC 2018 [12] referring to the municipalities of Benevento (soil type B and T_1 category) and Tramutola (soil type C and T_1 category). Three distinct limit states characterized by different return periods of the design earthquakes are considered: (i) the first limit state is associated with life safety requirement (LLS) and a 10 % probability of exceedance during the reference life of the structure V_R, which corresponds to a return period T_R of the design earthquake of 475 years; (ii) the second limit state refers to non-collapse requirement (CLS1) and a 5 % probability of exceedance during V_R, corresponding to a T_R of 975 years; (iii) the third limit state is referred again to non-collapse requirement (CLS2) but with a 2.5 % probability of exceedance during V_R, which results in a T_R of 1950 years. The choice of this latter limit state is in line with the indications of ASCE/SEI 41-17 [27] and allows to extend the investigation to a broader range of PGAs, in line with the ongoing revision of the Eurocode which is aiming to propose a revision of the γ-factor in order to increase the structural reliability. Table 3 lists the PGAs at either site for the selected return periods.

For each site and limit state, a suite of 7 independent bidirectional natural ground motion records are selected from the European Ground Motion Database [66] using the software Rexel [67]. The acceleration time-histories are scaled in magnitude in order to match the target elastic spectrum at 5 % equivalent viscous damping ratio defined by the NTC 2018 [12] for an ordinary structure (functional class cu = II) with a nominal life V_N = 50 years in the range of periods [0.15–2.00] s, with lower and upper tolerances of −10 % and +30 %, respectively. The magnitude (Mw) of the seismic events is selected within the interval

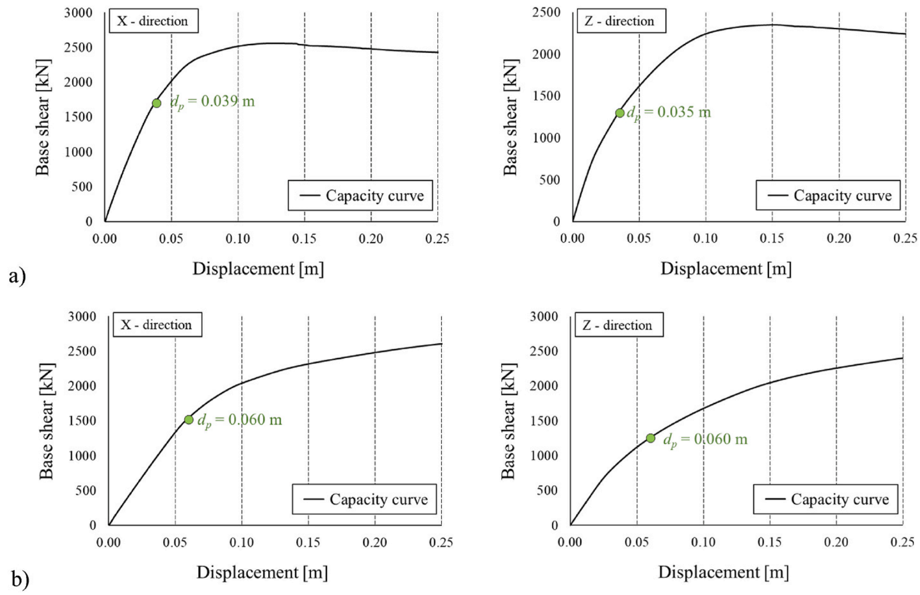

Fig. 5. Capacity curves with displacement limit values d_p in X-direction and Z-direction for (a) 3-story building and (b) 6-story building.

Table 3
PGAs for the selected return periods.

	$PGA_{T_R 475y}$ [m/s^2]	$PGA_{T_R 975y}$ [m/s^2]	$PGA_{T_R 1950y}$ [m/s^2]
Benevento	2.94	3.69	4.81
Tramutola	3.41	4.14	4.85

[5–7], with an epicentral distance (R_{ep}) in the range 0–30 km. Details of the selected records are provided in Figs. 6 and 7.

For each bidirectional ground motion, two analyses are performed by switching the two components of the earthquake excitation with respect to the main plan directions of the building, to account for possible directionality effects.

6. Results and discussions

6.1. Damper reliability and statistical evaluation of the amplification factor

The results of the analyses are first evaluated in terms of the displacement demand of the dampers at the three hazard levels considered in the study. As an example, Fig. 8(a) reports the hysteretic force – displacement response of a damper with ductility $\mu_D = 16$ encased in a bracing system with stiffness ratio $K_B/K_D = 2$ installed at the base floor of the 3-story building subjected to the 000042 accelerogram. It must be underlined that this accelerogram was included, with different Scale Factors, in every set of ground motions selected for

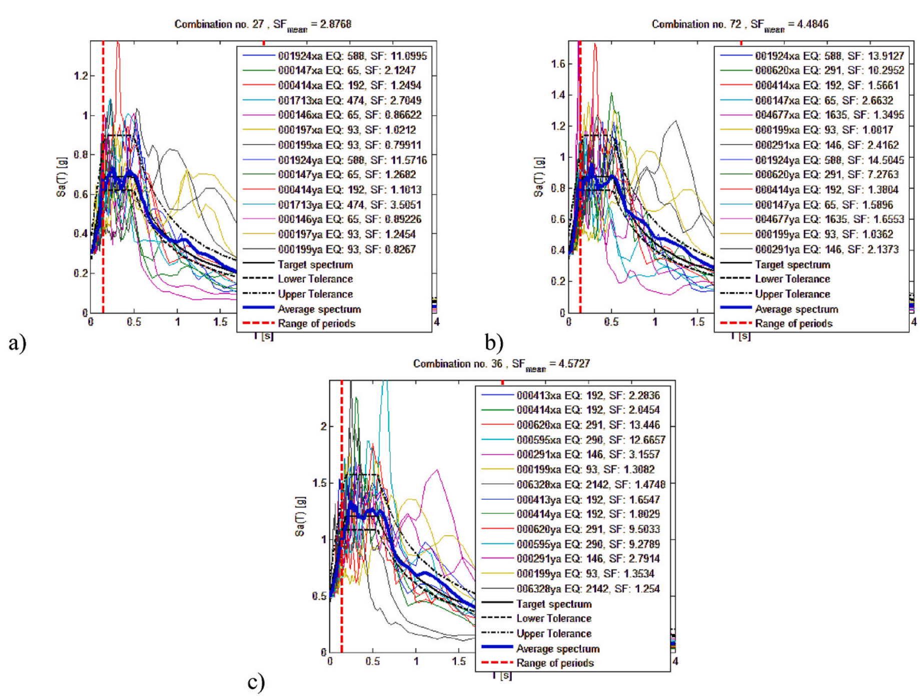

Fig. 6. Scaled ground motion spectra and target spectra for the municipality of Benevento and return period (a) T_R = 475 years, (b) T_R = 975 years and (c) T_R = 1950 years. SF: scale factor.

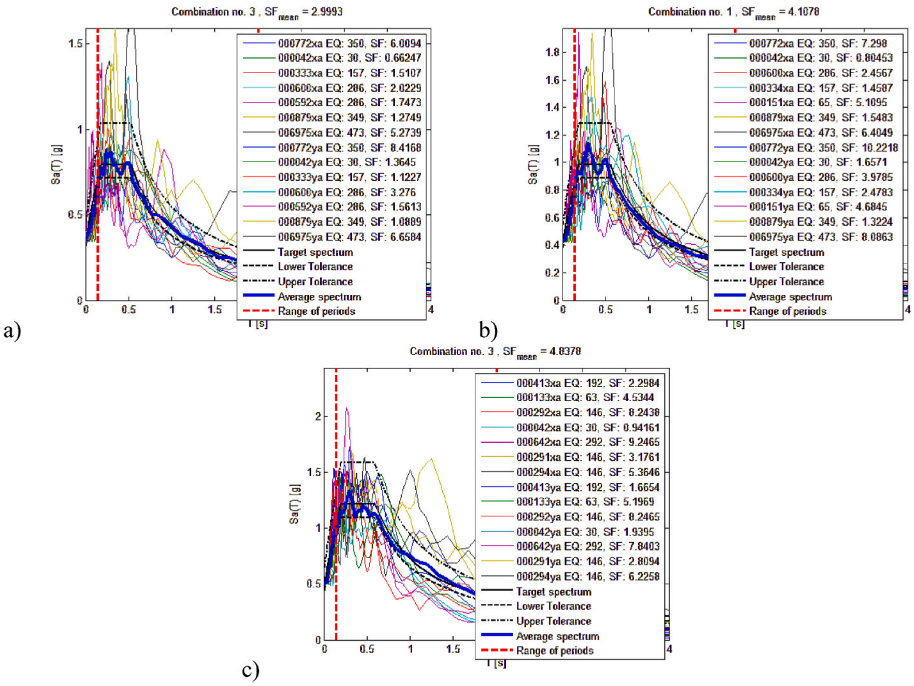

Fig. 7. Scaled ground motion spectra and target spectra for the municipality of Tramutola and return period (a) T_R = 475 years, (b) T_R = 975 years and (c) T_R = 1950 years.

the three hazard levels at the site of Tramutola. Only the hysteretic plots relevant to the most stressed damper of the 3-story building are reported for sake of conciseness, as similar trends were observed for the 6-story building as well, and for both sites. As shown in the diagrams, the maximum seismic displacement d_{bd} increases with the seismic intensity, and counts 0.0064 m at LLS, 0.0105 m at CLS1 and 0.0167 m at CLS2, with an increase of 1.65 and 2.70 times, respectively. In accordance with the assumed elastic-perfectly plastic behavior of the damper (Fig. 4), the damper force is independent of the deformation.

In order to highlight the contribution of the damper as compared to the stiffening effect of the bracing system in which the damper is encased, the plots of Fig. 8(a) can be compared to those of Fig. 8(b) and (c) which are relevant to damped brace systems at the ground floor of the 3-story building with different μ_D and K_B/K_D ratio. As expected, for an assigned damper increasing the stiffness of the encasing brace leads to an increase in the deformation of the device during the earthquake: in the example given in Fig. 8(b) relevant to a bracing system with K_B/K_D = 5, the maximum damper displacements are 0.0082 m at LLS, 0.0139 m at CLS1 and 0.0222 m at CLS2. However, it must be emphasized that, even if there is a general increase in the damper deformation by increasing K_B/K_D = 5, the over-demand for the damper has not a comparable change: the amplification of the LLS deformation is amplified by 1.65 (at CLS1) and 2.61 (at CLS2) times when K_B/K_D = 2, and by 1.70 (at CLS1) and by 2.71 (at CLS2) when K_B/K_D = 5, respectively.

On the contrary, reducing the ductility μ_D does not significantly affect the damper deformation. At LLS the damper displacement d_{bd} is defined by the target structural displacement d_p which is the object of the retrofit design and by the K_B/K_D ratio, whichever μ_D. By comparing Fig. 8(a) and (c) relevant to dampers with μ_D = 16 and μ_D = 4, respectively, encased in a bracing system with stiffness ratio K_B/K_D = 2, the influence of μ_D is noticed to be irrelevant also at CLS1 and CLS2: with μ_D = 4 the damper deformation counts 0.0107 m at CLS1 and 0.0165 m at CLS2, and the relevant over-demands are substantially equivalent to those calculated for the damper with μ_D = 16. This behavior can be explained by noticing that the equivalent damping ratio of the damped braces with μ_D = 4 is already high (ξ_{DB} = 49 %), and increasing the ductility to μ_D = 16 does not lead to a significant increase in ξ_{DB}; on the other hand, dampers with lower μ_D develop higher forces, e.g., in the example V_y = 818 kN (μ_D = 4) vs. V_y = 632 kN (μ_D = 16), which must be taken into account for the local strengthening of the columns connected to the brace system.

The damper over-demand at ground motions of higher intensity than those considered at BDE is evaluated by means of the amplification index β, defined as the ratio between the damper displacement $d_{bd,975years}$ or $d_{bd,1950years}$ calculated at hazard levels corresponding to CLS1 and CLS2, respectively, and the displacement $d_{bd,475years}$ at LLS, that is assumed as reference. In order to distinguish between the two return periods, the labels β_1 and β_2 are introduced, which refer to the ratios $\frac{d_{bd,975years}}{d_{bd,475years}}$ and $\frac{d_{bd,1950years}}{d_{bd,475years}}$ respectively. Figs. 9–12 report, for the two case-study structures, the values of β_1 and β_2 for the dampers at each floor of the building, calculated for different values of μ_{DB} (where μ_{DB} refers to the design value at LLS). For the 3-story structure (Figs. 9 and 10), the diagrams show the tendency of both β_1 and β_2 to increase with increasing of μ_{DB}. This trend is especially apparent for the buildings located in Benevento (Fig. 9), where β_1 and β_2 achieve their maxima at the first floor. In particular, β_1 increases from a minimum of 1.46 for μ_{DB} = 3 to a maximum of 2.35 for μ_{DB} = 13.5, while β_2 increases from 2.52 to 5.72 over the same range of μ_{DB}. Lower amplifications are obtained for the buildings in Tramutola (Fig. 10), especially at the highest hazard level, where β_2 rises from 2.3 for μ_{DB} = 3 to 2.67 for μ_{DB} = 13.5.

In the 6-story building (Figs. 11 and 12), the amplification index is less sensitive to μ_{DB}. In particular, by referring to the 4th story of the building in Benevento that shows the maxima of β_1 and β_2, there is only a slight increase (from 1.78 to 1.96 for β_1, and from 3.18 to 3.53 for β_2) increasing μ_{DB} from 5 to 13.5, while for the building in Tramutola the maxima of β_1 and β_2 tend to remain constant or even to decrease.

By recalling the results presented in Fig. 8(a) and (b), i.e., stiffer braces are shown to increase the maximum displacement of the dampers, but do not modify significantly the over-demand if compared to the displacement at LLS. Similar results were obtained for all the cases considered in the analyses, but are not reported for conciseness. Therefore, it is concluded that the stiffness ratio K_B/K_D does not affect the reliability of the results of the reliability analysis.

The values of β_1 and β_2 at each floor are used to build the lognormal

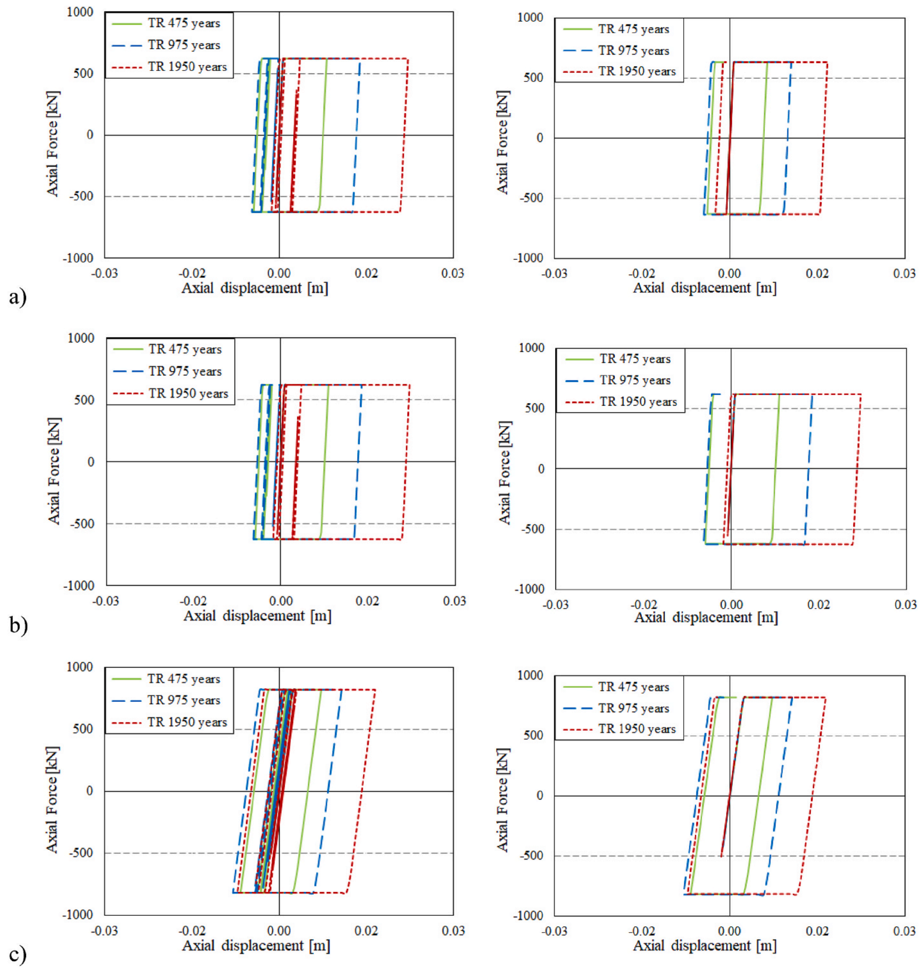

Fig. 8. Plots of hysteretic force – displacement cycles of a damper at the ground floor of the 3-story building subjected to the 000042 ground motion time-history for three hazard levels: (a) $\mu_D = 16$ and $K_B/K_D = 2$; (b) $\mu_D = 16$ and $K_B/K_D = 5$; (c) $\mu_D = 4$ and $K_B/K_D = 2$. Panels on the left: complete cycles; panels on the right: detail of the first cycle.

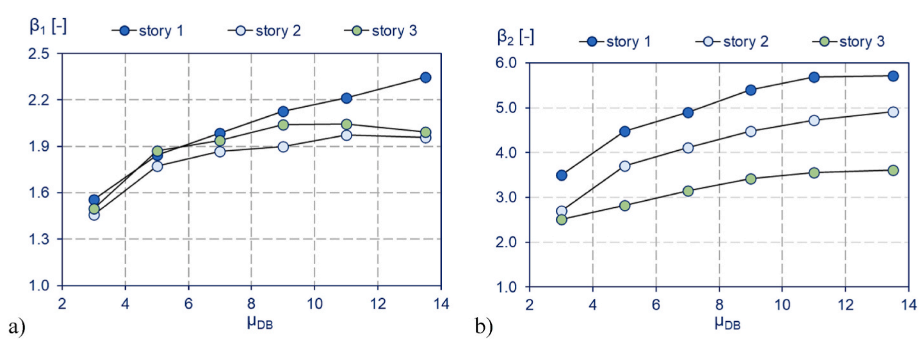

Fig. 9. β_1 and β_2 amplification indexes for 3-story building, site of Benevento.

distributions of the probability density function (pdf) to statistically estimate the amplification factor from the analyses. The pdf curves are shown in Figs. 13 and 14, while Table 4 reports the values of β_1 and β_2 referred to the 95 % fractile. Based on these results, the reliability at 95 % of the hysteretic dampers installed in either building and in either site is guaranteed if they are designed for displacements equal to 1.6 ÷ 2.3 $d_{bd,475years}$ for the T_R = 975 years hazard level (CLS1), and for displacements equal to 2.7 ÷ 5.6 $d_{bd,475years}$ for the T_R = 1950 years hazard level (CLS2). It is worth noting that even at the less severe CLS1 the amplification of the design displacement largely exceeds the values recommended in current standards, i.e. 1.1 as per EN 15129 [13], 1.2 as per NTC [12] and 1.3 as per ASCE (SEI 41–2017) [27]. Therefore, hysteretic dampers designed for the BDE according to the current code would fail under a ground motion with intensity corresponding to T_R = 975 years.

In Fig. 15, the maxima values of the β indexes calculated for the two structures considering both sites are plotted with respect to the ratio between the PGAs of the Non-Collapse Limit States CLS1 and CLS2 and the design PGA for LLS.

For both buildings, disregarding a single data point, an almost linear dependency of the amplification index on the PGA ratio is apparent. The results of the 3-story building indeed show a larger dispersion compared

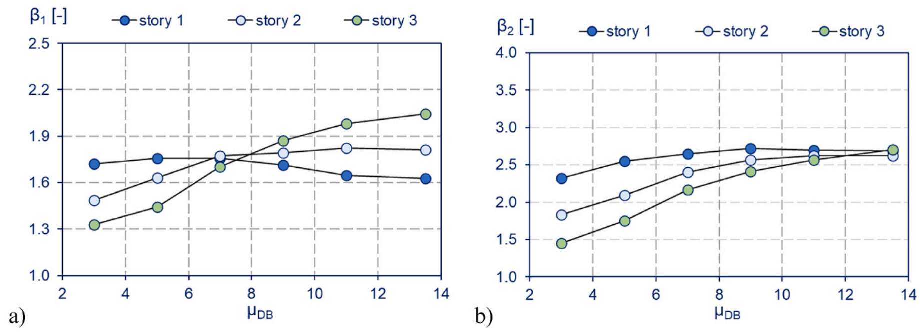

Fig. 10. β_1 and β_2 amplification indexes for 3-story building, site of Tramutola.

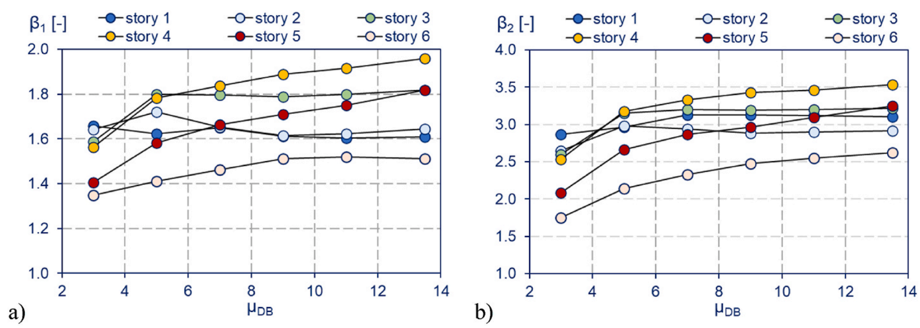

Fig. 11. β_1 and β_2 amplification indexes for 6-story building, site of Benevento.

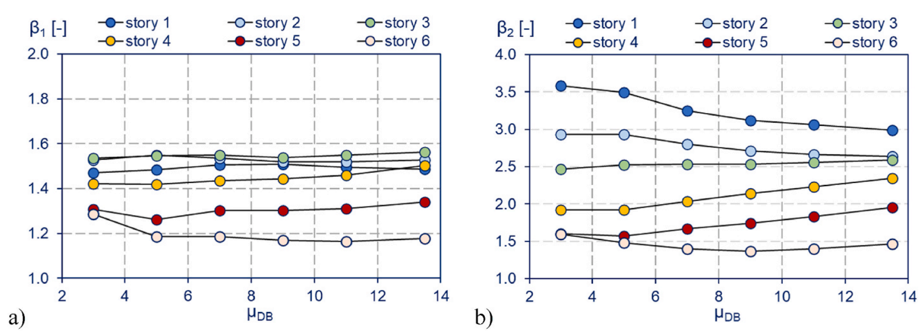

Fig. 12. β_1 and β_2 amplification indexes for 6-story building, site of Tramutola.

to the 6-story frame, especially for low damper ductility; however, these differences tend to decrease at larger PGAs, and when the PGA ratio is 1.64 the differences are within 10 %. On the other hand, for the 6-story building, disregarding the case $\mu_{DB} = 3$, the curves for different μ_{DB}s virtually overlap each other.

6.2. Structural reliability

The analysis of the structural reliability is performed under the assumption that the dampers are provided with sufficient capacity to accommodate the displacement demand at CLS1 and CLS2, and therefore they remain effective during the ground motions.

As an example, Fig. 16 shows the maximum displacement at each floor of the two case-study structures, placed in the municipality of Benevento and retrofitted with damped braces with either $\mu_{DB} = 11$ (corresponding to $\mu_D = 16$ and $K_B/K_D = 2$) or $\mu_{DB} = 13.5$ ($\mu_D = 16$ and $K_B/K_D = 5$), respectively, calculated from non-linear analyses considering the three hazard levels; similar results were obtained for either site for all μ_{DB}s. The plots reported in Fig. 16(a) and (b) show that, for both structures, the lateral displacement of each floor is practically unaffected by the K_B/K_D ratio. The target performance is met at the LLS, while at either CLS1 or CLS2 the displacement at the top of the building increases respectively by 1.9 times or 4.5 times with respect to the value at LLS for the 3-story building, and by 1.7 or 3.2 times for the 6-story building. It is worth recalling that increasing the K_B/K_D ratio leads to a higher level of plasticization of the dampers, but does not changes the over-demand if compared to the deformation at LLS.

The structural reliability of the retrofitted structures for seismic actions at MCE is performed by checking the resistance of the columns to the bending moment. The verification is performed in accordance with the provisions of NTC 2018 [12], which are similar to those of the Eurocode 2 [68], considering the influence of the axial load according to Eq. (5):

$$\left(\frac{M_{E_{yd}}}{M_{R_{yd}}}\right)^{\alpha} + \left(\frac{M_{E_{zd}}}{M_{R_{zd}}}\right)^{\alpha} \leq 1 \tag{5}$$

where $M_{E_{yd}}$, $M_{E_{zd}}$ are the acting bending moments about the axes of symmetry of the columns, $M_{R_{yd}}$, $M_{R_{zd}}$ are the corresponding resisting moments, and exponent α is determined according to the geometry of the column cross-section and to the ratio $\frac{N_{Ed}}{N_{R_{cd}}}$ between the acting axial

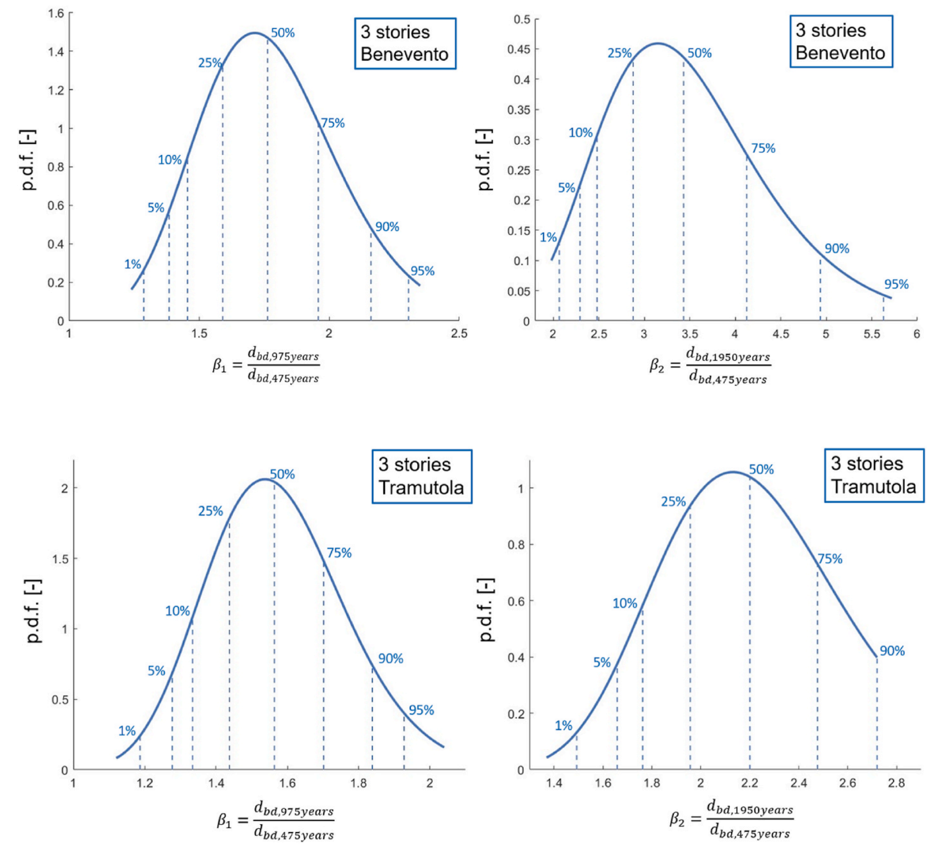

Fig. 13. Probability density functions of β_1 and β_2 for the 3-story building.

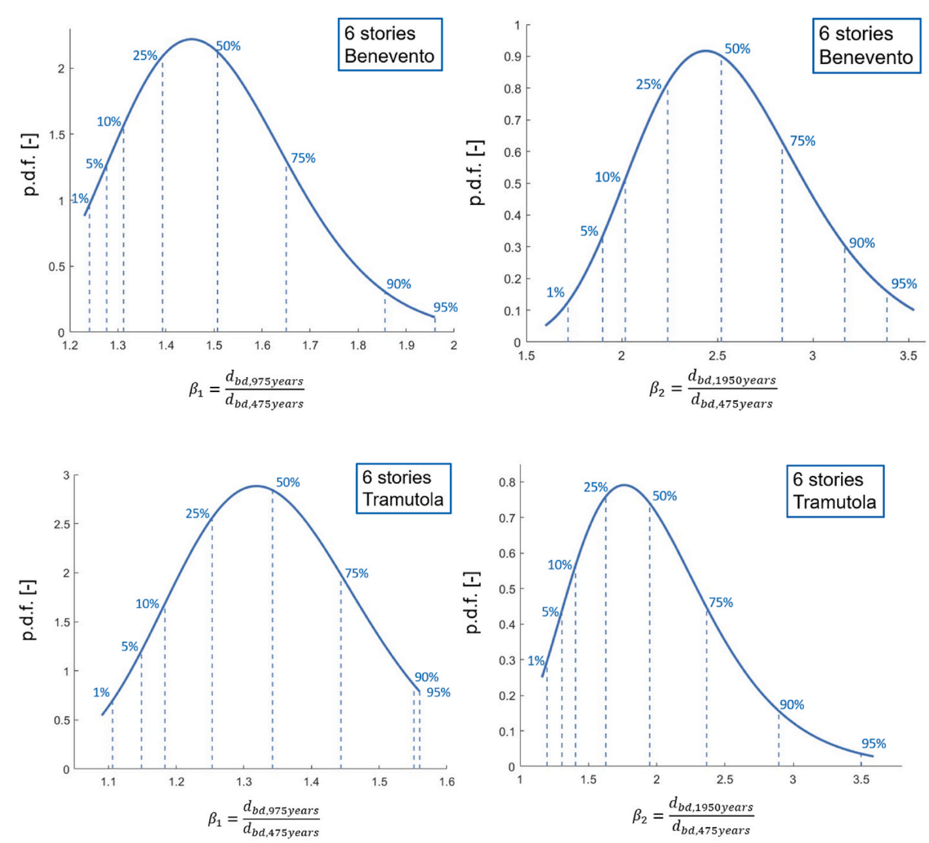

Fig. 14. Probability density functions of β_1 and β_2 for the 6-story building.

Table 4
Values of β_1 and β_2 referred to the 95 % fractile.

Case-study	*Site*	β_1	β_2
3-story	Benevento	2.31	5.63
	Tramutola	1.93	2.72
6-story	Benevento	1.96	3.39
	Tramutola	1.56	3.50

force N_{E_d} and the resisting axial force $N_{R_{cd}}$, as prescribed in Refs. [12, 68].

Figs. 17 and 18 report for either structure the number of columns at the ground floor for which the check is not verified (only the results relevant to the ground floor are reported for brevity since it is the story with the highest number of unverified columns). These cases are analyzed in relation with the ductility of the damped brace system and the seismic area.

The structural reliability increases by increasing the ductility of the damped brace system. Indeed, for both structures and both hazard levels the number of unverified columns decreases as μ_{DB} increases from $\mu_{DB} =$

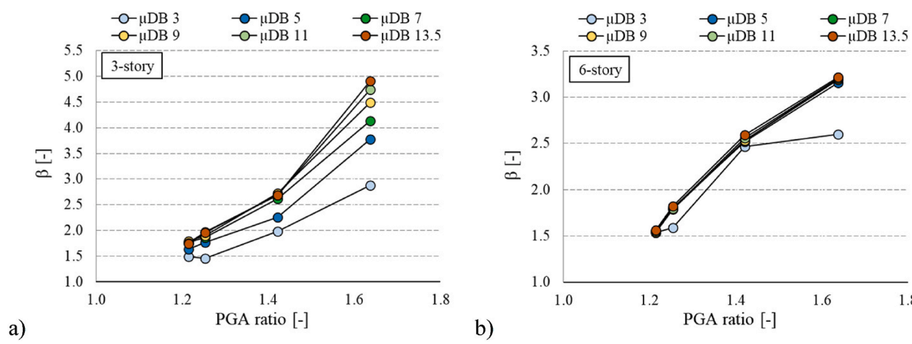

Fig. 15. Trend of β amplification indexes with respect to PGA ratio.

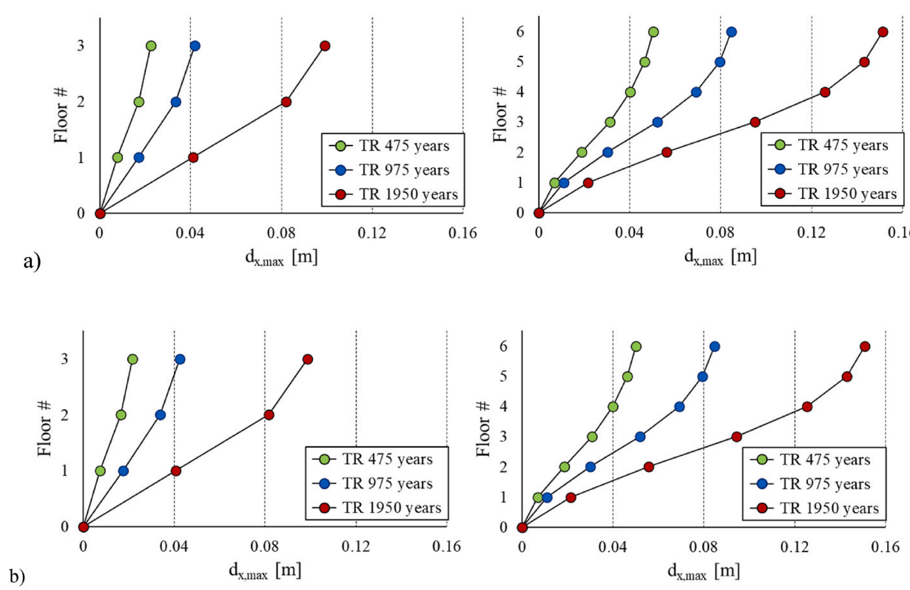

Fig. 16. Maximum displacement d_{max} at each floor of the retrofitted 3-story structure (a) and 6-story structure (b) placed in Benevento: (a) $\mu_D = 16$ and $K_B/K_D = 2$; (b) $\mu_D = 16$ and $K_B/K_D = 5$.

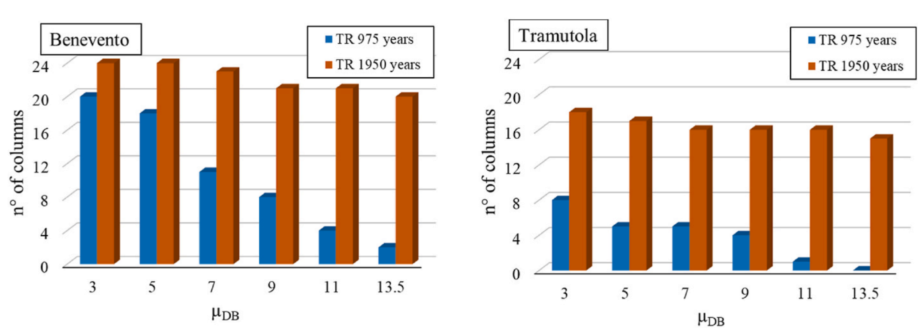

Fig. 17. Number of unverified columns at the ground floor of the 3-story structure.

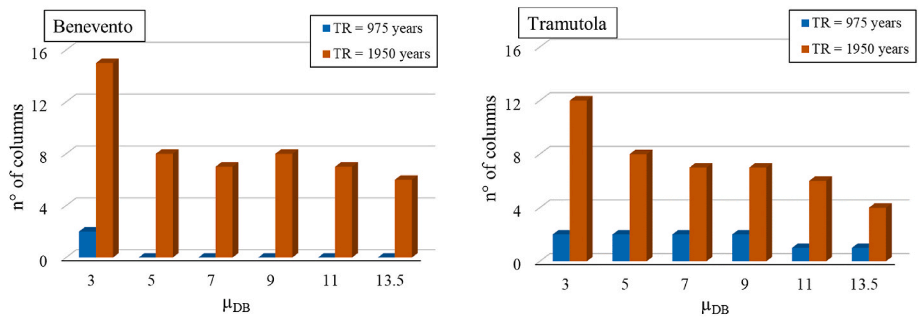

Fig. 18. Number of unverified columns at the ground floor of the 6-story structure.

3 to $\mu_{DB} = 13.5$. This is particularly apparent for the 3-story structure at CLS1, where the number of unverified columns diminishes from 20 for $\mu_{DB} = 3$ to only 2 for $\mu_{DB} = 13.5$ for the site of Benevento, and from 8 to 0 for the site of Tramutola, respectively. The dependency of the structural reliability upon μ_{DB} is less obvious at CLS2, since the number of unverified columns has only a small decrease over the considered range of ductility of the damped brace system.

The 6-story building shows a higher structural reliability since the number of unverified columns is considerably lower than that of the 3-story counterpart. Considering CLS1, in the building at Benevento the columns at the first floor are always verified but for the case $\mu_{DB} = 3$, where 2 columns are unverified; in the building at Tramutola there are 2 unverified columns for μ_{DB} spanning from 3 to 9, and 1 unverified column for μ_{DB} equal to 11 and 13.5. As expected, the number of unverified elements is larger at CLS2, but in this case increasing μ_{DB} from 3 to 5 produces a significant improvement in the structural response reducing the number of unchecked elements, and a tendency towards a further (but small) decrease of collapsed column is observed for high ductility levels.

7. Conclusions

Seismic Standards (e.g. Refs. [12,13,27]) require that anti-seismic devices for seismic isolation and energy dissipation must be designed to satisfy the performance requirements under the effects of the design seismic action (Basic Design Earthquake corresponding to Life Safety Limit State according to NTC 2018 [12]), and to resist, with an adequate degree of reliability, to earthquakes of higher intensity corresponding to Non-Collapse Limit States (Maximum Considered Earthquake). Therefore, the capacity of isolators and dampers is designed considering an appropriate reliability factor on the design displacement or design force. However, the recommended values for such reliability factors are not homogenous among the various Codes and the level of safety attainable through their use has not been sufficiently investigated.

The study presents a preliminary computational investigation of the reliability of RC structures retrofitted with hysteretic dampers considering two archetype buildings consisting of a low-rise and a medium-rise RC frame. The seismic upgrade of both structures is designed for a return period of 475 years in accordance with the Italian Building Code [12], and considering damped braces characterized by different ductility levels μ_{DB} and different stiffness ratios K_B/K_D. The retrofitted structures are then verified for two Non-Collapse Limit States with return periods of $T_R = 975$ and $T_R = 1950$ years respectively. The results are necessarily restricted to the response of the two simulated structures drawn from the literature. Nonetheless the study already highlights a first series of interesting observations and trends.

(1) The amplification factors prescribed for hysteretic dampers by current codes are largely under-conservative: for the two seismic scenarios considered in the study, amplifications of the design displacement up to 2.3 times for seismic actions with $T_R = 975$ years, and up to 5.6 for seismic actions with $T_R = 1950$ years were obtained, where the corresponding amplification factors proposed in EN15129 [13], Italian NTC 2018 [12] and ASCE/SEI 41 [27] Standards range from 1.1 to 1.3.
(2) The displacement demand for the dampers increased proportionally to the ratio between PGAs at the Maximum Considered and at the Basic Design Earthquake.
(3) On the other hand, the over-demand was practically independent of the damper ductility μ_{DB}, especially for the 6-story frame, as well as of the ratio between the stiffnesses of the bracing system and the damper K_B/K_D. This suggests that as far as the reliability of the device is concerned, neither the damper ductility nor the stiffness ratio is influencing.
(4) On the contrary, the structural reliability, evaluated by means of the number of unverified columns at the ground floor of the investigated buildings, increases with the ductility of the dampers. In addition, a certain effect of the structural system is also evident, as the 3-story building showed a larger number of unverified columns for same seismic input and ductility of the damped braces than the 6-story frame.

Though the study presents only a preliminary investigation considering only two case-study buildings and two seismic scenarios, the Authors deem that its value lies in the fact that for the first time the performance and reliability of hysteretic dampers, and of the structures where these devices are installed, is evaluated in a systematic approach, and it can be the basis for developing suggestions for revising the design prescriptions of seismic codes. It must be mentioned that the general validity of the work is not limited by the selected brace configuration, since it has been demonstrated that the effectiveness of the retrofit in achieving the performance objective is not dependent upon the bracing system configuration and structures with different bracing systems showed analogous responses in terms of inter-story drifts and floor accelerations [20].

The validity of the results presented in the study is confined to the examined cases and cannot be meant as general until it will be confirmed by further data. In future developments, the study will be extended to a wider range of building typologies (RC and steel structures) characterized by different number of stories, and the dependency of the results upon the selected seismic scenario will be tackled considering different sites, characterized by diverse topographies and soil conditions.

Funding

This work was funded by the Italian Department of Civil Protection (DPC) in the frame of the national Research Project DPC-ReLUIS 2022–2024 Work Package WP 15 "*Contributi normativi an isolamento e dissipazione*".

Declaration of competing interest

The authors declare that they have no known competing financial interests or personal relationships that could have appeared to influence the work reported in this paper.

Data availability

Data will be made available on request.

References

[1] Quaglini V, Pettorruso C, Bruschi E. Experimental and numerical assessment of prestressed lead extrusion dampers. Ing Sismica 2021;XXXVIII:46–69.

[2] Sedaghatnezhad H, Fallah A, Yazdi MM, Mohseni PK. Investigation of seismic coefficient factor for divergent bracing frame with TADAS damper utilizing the FEMA P695. J Inst Eng: Series A 2022 2022;103:263–70. https://doi.org/10.1007/s40030-021-00576-3.

[3] Quaglini V, Bruschi E. Controllo passivo mediante controventi dissipativi. Principi generali, requisiti normativi ed evoluzione dei principali dispositivi a comportamento dipendente dallo spostamento. Structural 2022;240:9. https://doi.org/10.12917/STRU240.09.

[4] Ponzo FC, Di Cesare A, Telesca A, Pavese A, Furinghetti M. Advanced modelling and risk analysis of RC buildings with sliding isolation systems designed by the Italian seismic code. Appl Sci 2021;11:1938. https://doi.org/10.3390/app11041938.

[5] Bruschi E, Quaglini V. Assessment of a novel hysteretic friction damper for the seismic retrofit of reinforced concrete frame structures. Structures 2022;46:793–811. https://doi.org/10.1016/j.istruc.2022.10.113.

[6] Bruschi E, Zoccolini L, Cattaneo S, Quaglini V. Experimental characterization, modelling and numerical evaluation of a novel friction damper for the seismic upgrade of existing buildings. Materials 2023;16:1933. https://doi.org/10.3390/ma16051933.

[7] Martínez-Rueda JE. On the evolution of energy dissipation devices for seismic design. Earthq Spectra 2022;18(2):309–46. https://doi.org/10.1193/1.1494434.

[8] Cardone D, Conte N, Dall'Asta A, Di Cesare A, Flora A, Lamarucciola N, Micozzi F, Ponzo FC, Ragni L. RINTC-E Project: the seismic risk of existing Italian RC buildings retrofitted with seismic isolation. In: 7th ECCOMAS thematic Conference on computational Methods in structural Dynamics and earthquake engineering. Greece: Crete; 2019. June 24-26.

[9] Christopoulos C, Filiatrault A. Principles of passive supplemental damping and seismic isolation. first ed. Pavia: IUSS Press; 2006.

[10] CEN (European Committee for Standardization). Design of structures for earthquake resistance – Part 1: general rules, seismic actions and rules for building. 2005. EN 1998–1 Eurocode 8.

[11] CEN (European Committee for Standardization). Design of structures for earthquake resistance – Part 2: bridges. EN 1998–2 Eurocode 8. 2005.

[12] CSLLPP (Consiglio Superiore dei Lavori Pubblici). 17 gennaio 2018 in materia di "norme tecniche per le costruzioni". Gazzetta ufficiale n.42 del 20 febbraio 2018, Supplemento ordinario n.8. D.M. Roma: Ministero delle Infrastrutture e dei trasporti; 2018. Italian.

[13] CEN (European Committee for Standardization). European committee for standardization. 2009. EN 15129. Anti-seismic devices. Brussels.

[14] Bruschi E, Quaglini V, Calvi PM. A simplified design procedure for seismic upgrade of frame structures equipped with hysteretic dampers. Eng Struct 2021;251:e113504. https://doi.org/10.1016/j.engstruct.2021.113504.

[15] Quaglini V, Bruschi E, Pettorruso C. Dimensionamento di dispositivi dissipativi per la riabilitazione sismica di strutture intelaiate. Structural 2021;e237. https://doi.org/10.12917/STRU237.25.

[16] Bruschi E, Quaglini V, Calvi PM. A simplified design procedure to improve the seismic performance of RC framed buildings with hysteretic damped braces. In: New metropolitan perspectives 2022 - 5th international symposium "post COVID dynamics: green and digital transition, between metropolitan and return to villages' perspectives", reggio calabria, Italy, 25-27 may, ISBN 978-3-031-06825-6. p. 2173–82. Volume 482 LNNS.

[17] Bruschi E, Quaglini V, Zoccolini L. Control of the seismic response of steel-framed buildings by using supplementary energy dissipation devices. Appl Sci 2023;13(4):2063. https://doi.org/10.3390/app13042063.

[18] Mazza F, Vulcano A. Displacement-Based Design procedure of damped braces for the seismic retrofitting of RC framed buildings. Bull Earthq Eng 2015;13:2121–43. https://doi.org/10.1007/s10518-014-9709-7.

[19] Mazza F, Mazza M, Vulcano A. Displacement-Based seismic Design of hysteretic damped braces for retrofitting in-elevation irregular RC framed buildings. Soil Dynam Earthq Eng 2015;69:115–24. https://doi.org/10.1016/j.soildyn.2014.10.029.

[20] Di Cesare A, Ponzo FC. Seismic retrofit of reinforced concrete frame buildings with hysteretic bracing systems: design procedure and behaviour factor. Shock Vib 2017:e2639361. https://doi.org/10.1155/2017/2639361.

[21] Nuzzo I, Losanno D, Caterino N. Seismic design and retrofit of frames structures with hysteretic dampers: a simplified displacement-based procedure. Bull Earthq Eng 2019;17:2787–819. https://doi.org/10.1007/s10518-019-00558-8.

[22] Scozzese F, Gioiella L, Dall'Asta A, Ragni L, Tubaldi E. Influence of viscous dampers ultimate capacity on the seismic reliability of building structures. Struct Saf 2021;91:102096. https://doi.org/10.1016/j.strusafe.2021.102096. ISSN 0167-4730.

[23] Sorace S, Terenzi G, Fadi F. Shaking table and numerical seismic performance evaluation of fluid viscous-dissipative bracing system. Earthq Spectra 2012;28(4). https://doi.org/10.1193/1.4000083.

[24] Terenzi G. Energy-based design criterion of dissipative bracing systems for the seismic retrofit of frame structures. Appl Sci 2018;8:268. https://doi.org/10.3390/app8020268.

[25] Terenzi G, Costoli I, Sorace S. Activation control extension of a design method of fluid viscous dissipative bracing systems. Bull Earthq Eng 2020;18:4017–38. https://doi.org/10.1007/s10518-020-00849-5.

[26] Quaglini V, Gandelli E, Dubini P, Limongelli MP. Total displacement of curved surface sliders under nonseismic and seismic actions: a parametric study. Struct Control Health Monit 2017;24(12):e2031. https://doi.org/10.1002/stc.2031.

[27] American Society of Civil Engineers. Seismic evaluation and retrofit of existing buildings: ASCE standard ASCE/SEI 41-17. American Society of Civil Engineers; 2017.

[28] Quaglini V, Pettorruso C, Bruschi E. Design and experimental assessment of a prestressed lead damper with straight shaft for seismic protection of structures. Geosci 2022;12:182. https://doi.org/10.3390/geosciences12050182.

[29] Quaglini V, Pettorruso C, Bruschi E. Supplemental energy dissipation with prestressed lead extrusion dampers (P-led): experiments and modeling. In: 8th ECCOMAS thematic conference on computational methods in structural dynamics and earthquake engineering, athens, Greece, 28–30 june; 2021.

[30] Quaglini V, Bruschi E, Pettorruso C, Sartori M. Design and experimental assessment of a novel damper with high endurance to seismic loads. Procedia Struct Integr 2023;44(C):1451–7. https://doi.org/10.1016/j.prostr.2023.01.186.

[31] Di Cesare A, Ponzo FC, Nigro D. Assessment of the performance of hysteretic energy dissipation bracing systems. Bull Earthq Eng 2014;12(6):2777–96. https://doi.org/10.1007/s10518-014-9623-z.

[32] Bruschi E, Quaglini V. Numerical investigation on the seismic performance of a RC framed building equipped with a novel Prestressed LEad Damper with Straight Shaft. Procedia Struct Integr 2023;44(C):1443–50. https://doi.org/10.1016/j.prostr.2023.01.185.

[33] Quaglini V, Gandelli E, Dubini P. Experimental investigation of the re-centring capability of curved surface sliders. Struct Control Health Monit 2016;24(2):e1870. https://doi.org/10.1002/stc.1870.

[34] Gandelli E, De Domenico D, Dubini P, Besio M, Bruschi E, Quaglini V. Influence of the breakaway friction on the seismic response of buildings isolated with curved surface sliders: parametric study and design recommendations. Structures 2020;27:788–812. https://doi.org/10.1016/j.istruc.2020.06.035.

[35] Gandelli E, Quaglini V. Effect of the static coefficient of friction of curved surface sliders on the response of an isolated building. J Earthq Eng 2018;24(9):1361–89. https://doi.org/10.1080/13632469.2018.1467353.

[36] Gandelli E, Quaglini V, Dubini P, Limongelli MP, Capolongo S. Seismic isolation retrofit of hospital buildings with focus on non-structural components. Ing Sismica 2018;35(4):20–56.

[37] Cardone D, Viggiani LRS, Perrone G, Telesca A, Di Cesare A, Ponzo FC, Ragni L, Micozzi F, Dall'Asta A, Furinghetti M, Pavese A. Modelling and seismic response analysis of existing Italian residential rc buildings retrofitted by seismic isolation. J Earthq Eng 2023;27(4):1069–93. https://doi.org/10.1080/13632469.2022.2036271.

[38] Di Cesare A, Ponzo FC, Telesca A. Improving the earthquake resilience of isolated buildings with double concave curved surface sliders. Eng Struct 2021;228:111498. https://doi.org/10.1016/j.engstruct.2020.111498.

[39] Di Cesare A, Ponzo FC, Telesca A. Mechanical model of the over-stroke displacement behaviour for double concave surface slider anti-seismic devices. Front Built Environ 2022;8:1083266. https://doi.org/10.3389/fbuil.2022.1083266.

[40] Zayas V, Mahin S, Constantinou MC. Safe and unsafe seismically isolated structures. PEER report No. 20016-01. Berkeley, CA, USA: Pacific Earthquake Engineering Research Center; 2016.

[41] Furinghetti M, Lanese I, Pavese A. Experimental hybrid simulation of severe aftershocks chains on buildings equipped with curved surface slider devices. Bldg 2022;12:1255. https://doi.org/10.3390/buildings12081255L.

[42] Furinghetti M, Yang T, Calvi PM, Pavese A. Experimental evaluation of extra-stroke displacement capacity for Curved Surface Slider devices. Soil Dynam Earthq Eng 2021;146:106752. https://doi.org/10.1016/j.soildyn.2021.106752.

[43] Cilsalar H, Constantinou MC. Parametric study of seismic collapse performance of lightweight buildings with spherical deformable rolling isolation system. Bull Earthq Eng 2020;18(4):1475–98. https://doi.org/10.1007/s10518-019-00753-7.

[44] Kitayama S, Constantinou MC. Effect of displacement restraint on the collapse performance of seismically isolated buildings. Bull Earthq Eng 2019;17(5):2767–86. https://doi.org/10.1007/s10518-019-00554-y.

[45] Kitayama S, Constantinou MC. Collapse performance of seismically isolated buildings designed by the procedures of ASCE/SEI 7. Eng Struct 2018;164:243–58. https://doi.org/10.1016/j.engstruct.2018.03.008.

[46] Di Cesare A, Ponzo FC. Effect of over-stroke capacity of curved surface sliders on the collapse safety of seismically isolated buildings. Lect Notes in Civ Eng 2023;309 LNCE:254–63.

[47] Ragni L, Cardone D, Conte N, Dall'Asta A, Di Cesare A, Flora A, Leccese G, Micozzi F, Ponzo FC. Modelling and seismic response analysis of Italian code-conforming base-isolated buildings. J Earthq Eng 2018;22(Suppl. 2):198–230. https://doi.org/10.1080/13632469.2018.1527263.

[48] Khoshkalam M, Mortezagholi MH, Zahrai SM. Proposed modification for ADAS damper to eliminate axial force and improve seismic performance. J Earthq Eng 2022;26(10):5130–52. https://doi.org/10.1080/13632469.2020.1859419.
[49] Terenzi G, Sorace S, Fuso E. Stiffening effects-controlling sizing procedure of ADAS dampers in seismic retrofit of frame structures. Front Built Environ 2023;9. https://doi.org/10.1080/13632469.2020.1859419.
[50] CRESME Ricerche. Incentivi e riduzione del rischio sismico in Italia. Ingegneria Sismica Italiana; 2020. Italian.
[51] Faleschini F, Zanini MA, Toska K. Seismic reliability assessment of code-conforming reinforced concrete buildings made with electric arc furnace slag aggregates. Eng Struct 2019;195:324–39. https://doi.org/10.1016/j.engstruct.2019.05.083.
[52] OPCM 3274. Primi elementi in materia di criteri generali per la classificazione sismica del territorio nazionale e di normative tecniche per le costruzioni in zona sismica. Ordinanza delPresidente del Consiglio dei Ministri n. 3274. 2003 [in Italian].
[53] Castaldo P, Tubaldi E, Selvi F, Gioiella L. Seismic performance of an existing RC structure retrofitted with buckling restrained braces. J Build Eng 2021;33:101688. https://doi.org/10.1016/j.jobe.2020.101688.
[54] Gandelli E, Taras A, Disti J, Quaglini V. Seismic retrofit of hospitals by means of hysteretic braces: influence on acceleration-sensitive non-structural components. Front Built Environ 2019;5(100). https://doi.org/10.3389/fbuil.2019.00100.
[55] McKenna F, Fenves GL, Scott MH. Open system for earthquake engineering simulation. Berkeley, CA: PEER Report; 2000.
[56] OpenSeesWiki online manual. Available online at: https://opensees.berkeley.edu/wiki/index.php/Main_Page [last access: April 2021].
[57] Scott MH, Fenves GL. Plastic hinge integration methods for force-based beam-column elements. J Struct Eng 2006;132(2):244–52. https://doi.org/10.1061/(ASCE)0733-9445(2006)132:2(244).
[58] CEN (European Committee for Standardization). Design of structures for earthquake resistance – Part 3: assessment and retrofitting of buildings. EN 1998–3 Eurocode 8. 2005.
[59] Bruschi E, Calvi PM, Quaglini V. Concentrated plasticity modelling of RC frames in time-history analyses. Eng Struct 2021;243:112716. https://doi.org/10.1016/j.engstruct.2021.112716.
[60] Bruschi E, Quaglini V, Calvi PM. Numerical assessment of concentrated plasticity models of ductile RC frames in non-linear dynamic analyses. In: 2nd fib Italy YMG symposium on concrete and concrete structures, Rome, Italy, november 18-19; 2021.
[61] Menegotto M, Pinto PE. Method of analysis for cyclically loaded RC plane frames including changes in geometry and non-elastic behaviour of elements under combined normal force and bending. In: IABSE: symposium on resistance and ultimate deformability of structures acted on by well defined repeated loads; 1973. Final Report.
[62] Filippou FC, Popov EP, Bertero VV. Effects of bond deterioration on hysteretic behavior of reinforced concrete joints, report EERC 83-19, *earthquake engineering research center*. Berkeley: University of California; 1983.
[63] Popovics S. A numerical approach to the complete stress-strain curve of concrete. Cement Concr Res 1973;3(5):583–99.
[64] Barbagallo F, Bosco M, Marino E, Rossi P. On the fibre modelling of beams in RC framed buildings with rigid diaphragm. Bull Earthq Eng 2020;18:189–210. https://doi.org/10.1007/s10518-019-00723-z.
[65] Mazzoni S, McKenna F, Scott MH, Fenves GL, Jeremic B. OpenSEES command language manual. *Pacific earthquake engineering research center*. Berkeley: University of California; 2003.
[66] Ambraseys N, Smit P, Sigbjornsson R, Suhadolc P, Margaris B. Internet-site for European strong-motion data. In: European commission, research-directorate general, environment and climate programme; 2002.
[67] Iervolino I, Galasso C, Cosenza E. REXEL: computer aided record selection for code-based seismic structural analysis. Bull Earthq Eng 2010;8:339–62. https://doi.org/10.1007/s10518-009-9146-1.
[68] CEN (European Committee for Standardization). Design of concrete structures – Part 1-1: general rules and rules for buildings. 2005. EN 1992–1-1 Eurocode 2.